SUPPLEMENTARY METHODS AND RESULTS

Paulsen et al. (2016) describe the samples and methods used for zircon separation, imaging, and U-Pb age analysis, the results of which are shown in Figure 2A for the 800-400 Ma U-Pb zircon population. For zircons large enough to accommodate another laser ablation spot, trace elements were measured using the same grain mount and the same LA-ICP-MS instrument, as described in Paulsen et al. (2016), in an effort to determine the source rock provenance of the igneous zircons. Where possible, laser spots were selected within the same zone, though the small size of the majority of zircons mostly precludes this possibility. A typical analysis consisted of: (1) 5 cleaning pulses, followed by (2) 17 seconds of washout, (3) 22 seconds of gas blank, and (4) 40 seconds ablation time followed by 5 seconds of waiting time before moving the stage. Two standards (either NIST610 or NIST612 synthetic glass standards) were dispersed every 30 analyses and used for drift correction. Zircon reference material 91500 was analyzed once in every block of samples as a secondary reference material. Drift correction and data reduction were carried out with the MATLAB-based SILLS software (Guillong et al., 2008), and trace element concentrations were normalized to a Si value of 151682 ppm (equivalent to the Si content in a grain that is 99% $ZrSiO_4$). Individual spot analysis error is difficult to quantify, but long-term laboratory reproducibility of homogenous glass standards indicates a precision of better than 5 rel. % for element >>LLOD. The trace element analytical data are reported in Table DR2.

One-way Means ANOVA (analysis of variance), was performed on the zircon trace element ratios used as proxies for various parameters related to arc evolution. This method was used to analyze the significance of differences among the groups' means and the variation. In our model the groups are trace element ratios for 20 Myr. increments used as a proxy for slab fluid addition (Fig. DR3), crustal input (Fig. DR4), and crustal thickness (Fig. DR5). We show additional examples of ratios for crustal input and thickness that also have similar patterns. The Sr/Y ratio is commonly utilized as a proxy for crustal thickness (e.g. Profeta et al., 2015; Chapman et al., 2015); however, the low abundance of Sr in zircon prevented accurate measurement for calculating this ratio. Therefore, we use other ratios (Yb/Gd and Y/Gd) for the crustal thickness proxy with elements that are in high abundance in zircons similar to Barth et al. (2013). All zircons are from granitoid parent rocks (see below) and were chosen from a restricted range of Hf contents (10-12k) to reduce the effects that melt compositional evolution might have on the ratios. The Hf range does not encompass the highest values in the dataset in an effort to specifically avoid the compositional influence of late-stage accessory phase crystallization. Importantly, there is no correlation between Hf and any of the trace element ratios, which demonstrates that melt evolution has a negligible effect on these ratios within the chosen range of Hf.

We applied the 'Long' classification and regression tree analysis (CART) to the zircon trace element data following Belousova et al. (2002), who showed that igneous parent rock type could be distinguished with >80% confidence for carbonatites (84%), syenites (100%), Ne-syenite and syenite pegmatites (93%), and dolerites (84%). Zircons from other granitoids (65-70% SiO_2, 70-75% SiO_2, >75% SiO_2, and larvikites, a high-k granitoid) were distinguished with a >80% confidence with further subdivision into SiO_2 classes commonly yielding misclassification primarily into higher or lower SiO_2 content and therefore lower confidence (Belousova et al., 2002). Basalts were distinguished with a 47% confidence (Belousova et al., 2002). We excluded zircons with U/Th ratios >10 ppm (n=47) from the CART analysis because the higher ratio can develop as a consequence of metamorphism (Hoskin and Schaltegger, 2003; Gehrels et al., 2009) and intra-crystalline age variation indicates cases where high U/Th ratios correlate with younger rims that surround older cores (Paulsen et al., 2016).

The 800-400 Ma U-Pb zircon ages are shown according to rock type in Figs. 2B and 3A-D on probability density diagrams (from Ludwig, 2003). These diagrams show each age and its uncertainty (for measurement error only) as a normal distribution, and sum all ages from a rock type into a single curve. The curves for the different rock types have been superimposed to identify the relative relationships between the probability peaks and lows. Dashed line in Fig. 3B represents relative probability age distribution of alkaline and carbonatite igneous crystallization ages from the Koettlitz Glacier alkaline suite (Worley et al., 1995; compiled ages from Cooper et al., 1997; Mellish et al., 2002; Read et al., 2002; Cottle and Cooper, 2006; Read, 2010; Martin et al., 2014; Hagen-Peter and Cottle, in press). White mica ^{40}Ar/^{39}Ar age data (n=200) in Fig. 3D are from Di Vincenzo et al. (2015). Dashed line in Fig. 3D represents relative probability age distribution yielded by the analysis of the subordinate 800-570 Ma white mica ^{40}Ar/^{39}Ar ages (n=35 of the cumulative 200 analyses) alone to vertically exaggerate the older portion of the probability curve (schematically indicated by white arrows) to better delineate relationships with respect to the granitoid peaks and troughs.

The age ranges and peak ages of clusters reported below were determined using the Age Pick Excel program (2009) of G. Gehrels available at the Arizona LaserChron Center (www.geo.arizona.edu/alc). The age ranges and peak ages require three or more age contributions at the 2-sigma level. The Age Pick program yields the numbers of grain ages that fall within an age range (not the number of analyses that make probability contributions to define the age range). The Age Pick program also yields the numbers of analyses that contribute to an age probability peak at the 2-sigma level. Probability peaks are required to have probability contributions from three or more overlapping analyses. We use the 2015 International Chronostratigraphic Chart timescale (Cohen et al. 2013, updated) where we discuss the age peaks below.

Granitoid Zircons

A total of 233 of 371 granitoid (granitoid >65% SiO_2 and larvikite in Belousova et al., 2002) U-Pb age analyses met acceptable concordance thresholds (Fig. 2B). The dominant age cluster yielded by the cumulative analysis ranges from 805–470 Ma (Tonian-Ordovician), contains 231 ages, and has 24 peaks in age probability at 792 Ma (n=6), 765 Ma (n=4), 753 Ma (n=4), 737 Ma (n=6), 703 Ma (n=22), 677 Ma (n=5), 657 (n=7), 650 (n=7), 638 (n=8), 625 (n=14), 605 (n=13), 593 (n=22), 579 (n=19), 572 (n=23), 559 (n=15), 538 (n=16), 517 (n=13), 512 (n=9), 505 (n=13), 493 (n=8), 488 (n=5), 481 (n=5), and 473 (n=4).

Mafic Zircons

A total of 58 dolerite (n=48/60) and basalt (n=10/18) U-Pb age analyses met acceptable concordance thresholds (Fig. 3A). The two dominant age clusters yielded by the cumulative analysis ranges from 610–572 Ma (Ediacaran; n=19) and from 565–533 Ma (Ediacaran-Cambrian; n=15) and include 7 peaks in age probability at 604 Ma (n=7), 596 Ma (n=3), 584 Ma (n=7), 576 Ma (n=7), 564 Ma (n=3), 555 Ma (n=6), and 547 Ma (n=9). Two additional clusters range from 692–672 Ma (Cryogenian; n=5 ages) and 650–634 Ma (Cryogenian-Ediacaran; n=5 ages) and include 5 age probability peaks at 687 Ma (n=3), 676 Ma (n=4), 647 Ma (n=4), and 641 Ma (n=5). One additional age probability peak also occurs at 628 Ma (n=3). Zircons in basalts are expected to be rare. Indeed, the basaltic zircons in Belousova et al. (2002) have the highest potential for being misclassified (47% confidence). However, these 'basaltic' zircons are more likely to be sourced from doleritic (plutonic) rocks given that most basalt will not be saturated in zircon until they are at low temperatures and mostly crystalline and the melt in equilibrium with those crystals has become evolved and the zirconium concentration has increased sufficiently (Hanchar and Watson, 2003). Hafnium is used as a proxy for melt evolution; increasing Hf with increasing SiO2. Therefore, the low Hf zircons that are classified as 'basaltic' would still likely be derived from a mafic magma similar in composition to a dolerite. We have included these 'basaltic' zircons for the sake of completeness for representing the mafic source rocks. Excluding these zircons does not significantly impact these results..

Carbonatite/Alkaline Zircons

A total of 53 carbonatite (n=22/27) and alkaline (syenite, n=30/34; Ne-syenite/syenite pegmatite, n=1/2) U-Pb age analyses met acceptable concordance thresholds (Fig. 3B). The dominant age cluster yielded by the cumulative analysis ranges from 629–546 Ma (Ediacaran), contains 45 ages, and has 8 peaks in age probability at 625 Ma (n=3), 605 Ma (n=9), 591 Ma (n=10), 584 Ma (n=11), 576 Ma (n=12), 566 (n=5), 558 Ma (n=8), and 552 Ma (n=9). These 591-576 Ma age probability peaks are similar to 593–572 Ma age probability peaks (584 Ma average) reported for alkaline (carbonatite and syenite) detrital zircons yielded by 4 Neogene beach sands and a Triassic sandstone in eastern Australia, which paleocurrent data suggest are derived from Wilkes Land just to the west of the NVL study area in Antarctica (Veevers et al., 2006; Veevers, 2007).

Metamorphic (U/Th>10) Zircons

A total of 33 of 42 metamorphic (U/Th>10) U-Pb age analyses met acceptable concordance thresholds (Fig. 3C). The 4 dominant age clusters yielded by the cumulative analysis range from 665–643 Ma (Cryogenian; n=4), 625–613 Ma (Ediacaran; n=3), 611–602 Ma (Ediacaran; n=3), and 540–528 Ma (Cambrian; n=3). These include 5 peaks in age probability at 658 Ma (n=3), 648 Ma (n=4), 618 Ma (n=4), 607 Ma (n=5), and 532 Ma (n=3). Four additional age probability peaks also occur at 628 Ma (n=3), 582 Ma (n=4), 556 Ma (n=3), and 546 Ma (n=4).

White Mica

A cumulative analyses of a total of 200 white mica $^{40}Ar/^{39}Ar$ age analyses from Di Vincenzo et al. (2014) yielded a dominant age cluster ranging from 633–477 Ma

(Ediacaran-Ordovician) (Fig. 3D). This cluster contains 188 ages and has 24 peaks in age probability at 631 Ma (n=3), 622 Ma (n=4), 614 Ma (n=5), 607 Ma (n=4), 604 Ma (n=5), 598 Ma (n=4), 593 Ma (n=6), 590 Ma (n=6), 584 Ma (n=6), 566 Ma (n=6), 561 Ma (n=12), 557 Ma (n=17), 552 Ma (n=17), 546 Ma (n=15), 533 Ma (n=22), 529 Ma (n=23), 524 Ma (n=22), 521 Ma (n=21), 515 Ma (n=17), 507 Ma (n=11), 503 Ma (n=7), 494 Ma (n=12), 485 Ma (n=16), and 480 Ma (n=9). One additional cluster ranges from 468–462 Ma (Ordovician; n=3 ages) and includes 1 age probability peak at 465 Ma (n=3).

REFERENCES CITED

Belousova, E.A., Griffin, W.L., O'Reilly, S.Y., and Fisher, N.I., 2002, Igneous zircon: trace element composition as an indicator of source rock type: Contributions to Mineralogy and Petrology, v. 143, p. 602-622, doi: 10.1007/s00410-002-0364-7.

Chapman, J.B., Ducea, M.N., Profeta, L., and DeCelles, P.G., 2015, Tracking changes in crustal thickness during orogenic evolution with Sr/Y; an example from the Western U.S. Cordillera: Geology, v. 43, p. 919–923.

Cohen, K.M., Finney, S.C., and Gibbard, P.L., 2013, updated. The ICS international chronostratigraphic chart: Episodes, v. 36, p. 199–204.

Cooper, A.F., Worley, B.A., Armstrong, R.A., and Price, R.C., 1997, Synorogenic alkaline and carbonatitic magmatism in the Transantarctic Mountains of South Victoria Land, Antarctica, *in* Ricci, C.A., ed., The Antarctic Region: Geological Evolution and Processes: Siena, Italy, Terra Antartica Publications, p. 245–252.

Cottle, J.M., and Cooper, A.F., 2006, Geology, geochemistry and geochronology of an A-type granite in the Mulock Glacier Area, southern Victoria Land, Antarctica: New Zealand Journal of Geology and Geophysics, v. 49, p. 191-202, doi: 10.1080/00288306.2006.9515159.

Crispini, L., L. Federico, and Capponi, G., 2014, Structure of the Millen Schist Belt (Antarctica): Clues for the tectonics of northern Victoria Land along the paleo-Pacific margin of Gondwana: Tectonics, v. 33, p. 420-440, doi: 10.1002/2013TC003414.

Di Vincenzo, G., Grande, A., and Rossetti, F., 2014, Paleozoic siliciclastic rocks from northern Victoria Land (Antarctica): Provenance, timing of deformation, and implications for the Antarctica-Australia connection: Geological Society of America Bulletin, v. 126, p. 1416-1438, doi:10.1130/B31034.1.

Estrada, S., Läufer, A.L., Eckelmann, K., Hofmann, M., Gärtner, A., and Linnemann, U., 2015, Continuous Neoproterozoic to Ordovician sedimentation at the East Gondwana margin — Implications from detrital zircons of the Ross Orogen in northern Victoria Land, Antarctica: Gondwana Research, (in press).

Federico, L., Capponi, G., and Crispini, L., 2006, The Ross orogeny of the Transantarctic Mountains: a northern Victoria Land perspective: International Journal of Earth Sciences, v. 95, p. 759-770, doi: 10.1007/s00531-005-0063-5.

Ferraccioli, F., Ferraccioli, F., Bozzo, E., and Capponi, G., 2002, Aeromagnetic and gravity anomaly constraints for an early Paleozoic subduction system of Victoria Land, Antarctica: Geophysical Research Letters, v. 29, p. 1-4, doi: 10.1029/2001GL014138.

Gehrels, G., et al., 2009, U-Th-Pb geochronology of the Coast Mountains batholith in north-coastal British Columbia: constraints on age and tectonic evolution: Geological Society of America Bulletin, v. 121, p. 1341–1361, doi: 10.1130/B26404.1.

Guillong, M., Meier, D., Allan, M., Heinrich, C., and Yardley, B., 2008, SILLS: a MATLAB-based program for the reduction of laser ablation ICP-MS data of homogeneous materials and inclusions: Mineralogical Association of Canada Short Course 40, p. 328-333.

Hagen-Peter, G., and Cottle, J.M., in press, Synchronous alkaline and subalkaline magmatism during the late Neoproterozoic–early Paleozoic Ross orogeny, Antarctica: Insights into magmatic sources and processes within a continental arc: Lithos, doi: 10.1016/j.lithos.2016.07.032.

Hall, C.E., Cooper, A F., and Parkinson, D.L., 1995, Early Cambrian carbonatite in Antarctica: Journal Geological Society London, v. 152, p. 721-728, doi: 10.1144/gsjgs.152.4.0721.

Hanchar, J. M., and Watson, E.B., 2003. Zircon saturation thermometry: Reviews in mineralogy and geochemistry, v. 53.1, p. 89-112.

Hoskin, P., and Schaltegger, U., 2003, The composition of zircon and igneous and metamorphic petrogenesis: In: Hanchar, J., Hoskin, P., (Eds.), Zircon: Reviews of Mineralogy and Geochemistry, v. 53, p. 27-62.

Kleinschmidt, G., and Tessensohn, F., 1987, Early Paleozoic westward directed subduction at the Pacific margin of Antarctica, *in* McKenzie, G.D., ed., Gondwana Six: Structure, Tectonics, and Geophysics. American Geophysical Union Geophysical Monograph, v. 40, p. 89-105.

Läufer, A.L., Kleinschmidt, G., Henjes-Kunst, F., Rossetti, F., and Faccenna, C., 2006, Geological Map of the Cape Adare Quadrangle Victoria Land, Antarctica: scale 1:250 000, 1 sheet.

Ludwig, K.R., 2003, Isoplot 3.00: Berkeley Geochronology Center, Special Publication 4, 70 p.

Martin, A.P., Cooper, A.F., Price, R.C., Turnbull, R.E., and Roberts, N.M.W., 2014, The petrology, geochronology, and significance of Granite Harbour Intrusive Complex xenoliths and outcrop sampled in western McMurdo Sound, Southern Victoria Land, Antarctic: New Zealand Journal of Geology and Geophysics, v. 58, p. 33-51, doi: 10.1080/00288306.2014.982660.

Mellish, S.D., Cooper, A.F. and Walker, N.W., 2002, The Panorama Pluton: a composite gabbro-monzodiorite, early Ross Orogeny intrusion in southern Victoria Land, Antarctica, *in* Gamble, J.A., Skinner, D.N.B., and Henrys, S., eds., Antarctica at the close of a millennium. The Royal Society of New Zealand Bulletin, v. 35, p. 129-141.

Paulsen, T.S., Deering, C., Sliwinski, J, Bachmann, O., and Guillong, M., 2016, Detrital zircon ages from the Ross Supergroup, north Victoria Land, Antarctica: Implications for the tectonostratigraphic evolution of the Pacific-Gondwana margin. Gondwana Research, v. 35, p. 79-96, doi:10.1016/j.gr.2016.04.001.

Profeta, L., Ducea, M.N., Chapman, J.B., Paterson, S.R., Gonzales, S.M.H., Kirsch, M., Petrescu, L., and DeCelles, P.G., 2015, Quantifying crustal thickness over time in magmatic arcs: Scientific Reports, v. 5, 17786, doi: 10.1038/srep17786.

Read, S.E., 2010, Koettlitz Glacier Alkaline Province: Late Neoproterozoic extensional magmatism in southern Victoria Land, Antarctica [Ph.D. thesis]: Dunedin: University of Otago, 630 p.

Read, S.E., Cooper, A.F., and Walker, N.W., 2002, Geochemistry and U-Pb geochronology of the Neoproterozoic-Cambrian Koettlitz Glacier Alkaline Province, Royal Society Range, Transantarctic Mountains, Antarctica, *in* Gamble, J.A., Skinner, D.N.B., and Henrys, S., eds., Antarctica at the close of a millennium: The Royal Society of New Zealand Bulletin, v. 35, p. 143-151.

Rocchi, S., Di Vincenzo, G., Ghezzo, C., and Nardini, I., 2009, Granite-lamprophyre connection in the latest stages of the Early Paleozoic Ross Orogeny (Victoria Land, Antarctica): Geological Society of America Bulletin, v. 121, p. 801-819, doi: 10.1130/B26342.1.

Stump, E., 1995, Ross orogen of the Transantarctic Mountains: New York, Cambridge University Press, 284 p.

Tessensohn, F., and Henjes-Kunst, F., 2005, Northern Victoria Land terranes, Antarctica: Far-travelled or local products?, *in* Vaughan, A.P.M., Leat, P.T., and Pankhurst, R.J., eds., Terrane Processes at the Margins of Gondwana: Geological Society of London Special Publication, v. 246, p. 275-291, doi: 10.1144/GSL.SP.2005.246.01.10

Veevers, J.J., 2007, Pan-Gondwanaland post-collisional extension marked by 650-500 Ma alkaline rocks and carbonatites and related detrital zircons: A review: Earth-Science Reviews, v. 83, p. 1-47, doi:10.1016/j.earscirev.2007.03.001.

Veevers, J.J., Belousova, E.A., Saeed, A., Sircombe, K., Cooper, A.F., and Read, S.E., 2006, Pan-Gondwanaland detrital zircons from Australia analysed for Hf- isotopes and trace elements reflect an ice-covered Antarctic provenance of 700-500 Ma age, TDM of 2.0-1.0 Ga, and alkaline affinity: Earth-Science Reviews, v. 76, p. 135-174, doi:10.1016/j.earscirev.2005.11.001.

Worley, B.A., Cooper, A.F., Hall, C.E., 1995, Petrogenesis of carbonate-bearing nepheline syenites and carbonatites from southern Victoria Land, Antarctica: Origin of carbon and the effects of calcite-graphite equilibrium: Lithos, v. 35, p. 183-199.

SUPPLEMENTARY FIGURE CAPTIONS

Supplementary Figure DR1. Simplified geologic map showing intrusive, sedimentary, and metamorphic basement rocks of the Ross orogen in north Victoria Land. Tectonostratigraphic differences across the area have led to the definition of the Wilson, Bowers, and Robertson Bay terranes, which are separated from their respective neighbors by regional fault zones (Crispini et al., 2014). Comparative analysis of detrital zircon age populations indicates that inboard stratigraphic successions (Wilson Terrane) and those located outboard of the East Antarctic craton (the Bowers and Robertson Bay terranes) have similar ~1200-950 Ma (Mesoproterozoic-Neoproterozoic) and ~700-490 Ma (late Neoproterozoic-Cambrian, Furongian) age populations (Paulsen et al., 2016; Estrada et al., in press). The affinity of the age populations of the sandstones to each other, as well as Gondwana sources and Pacific-Gondwana marginal stratigraphic belts, indicates that the outboard successions do not represent form exotic terranes that docked with Gondwana during the Ross orogeny and instead places the provinces in proximity to each other and within the peri-Gondwana realm during the late Neoproterozoic to Cambrian (Paulsen et al., 2016), in agreement with the conclusions reached by other authors (Kleinschmidt and Tessensohn, 1987; Ferraccioli et al., 2002; Tessensohn and Henjes-Kunst, 2005; Federico et al., 2006; Rocchi et al., 2011; Crispini et al., 2014; Estrada et al., in press). White stars indicate approximate locations of detrital zircon samples analyzed in this paper and black stars indicate approximate locations of detrital white mica samples analyzed by Di Vincenzo et al. (2015) for north Victoria Land. Figure compiled from Stump (1995) and Läufer et al. (2006).

Supplementary Figure DR2. Summary plot and statistics for One-way Means ANOVA (analysis of variance). Plot show means (center line in diamond) with 95% confidence intervals (upper and lower horizontal lines near apexes) for U/Yb through time. Time increments are 20 Myr. The ratios are assumed to increase with increasing slab-derived fluid addition due to the high mobility of U in fluids relative to other elements. The plot shows a broad peak in the U/Yb ratio over the period from 640-520 Ma.

Supplementary Figure DR3. Summary plots and statistics for One-way Means ANOVA (analysis of variance). Plots show means (center line in diamond) with 95% confidence intervals (upper and lower horizontal lines near apexes) for Th/U and Th/Yb through time. Time increments are 20 Myr. The ratios are assumed to increase with increasing crustal input due to enrichment in Th relative to other elements as the Proterozoic crust evolved. The plots show that a statistically significant difference exists between zircons that occur from 500-460 Ma and 620-560 Ma, and those through the rest of the period from 800-400 Ma.

Supplementary Figure DR4. Summary plots and statistics for One-way Means ANOVA (analysis of variance). Plots show means (center line in diamond) with 95% confidence intervals (upper and lower horizontal lines near apexes) for Yb/Gd and Y/Gd through time. Time increments are 20 Myr. The ratios are assumed to decrease with increasing crustal thickness due to the preferential incorporation of HREE (Yb) or Y into garnet. The presence of garnet in crustal magmas is indicative of high pressure. The plots show that a statistically significant difference exists between zircons that occur from 620-560 Ma compared to the rest of the period from 800-400 Ma. This is interpreted as a period where the thickest crust existed.

Supplementary Table DR1.

2016308_Table DR1.xlsx

Supplementary Figure DR1.

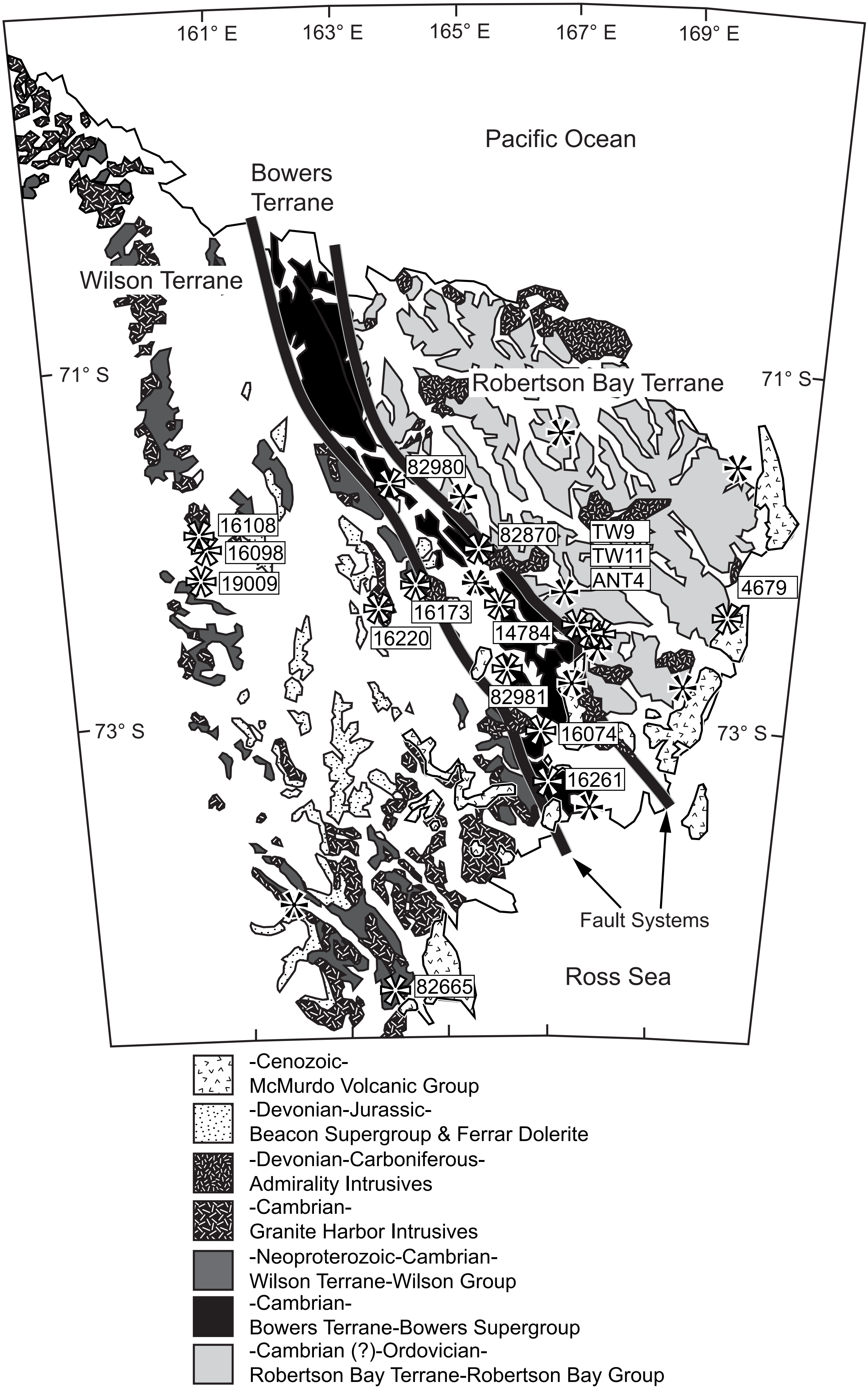

Supplementary Figure DR2.

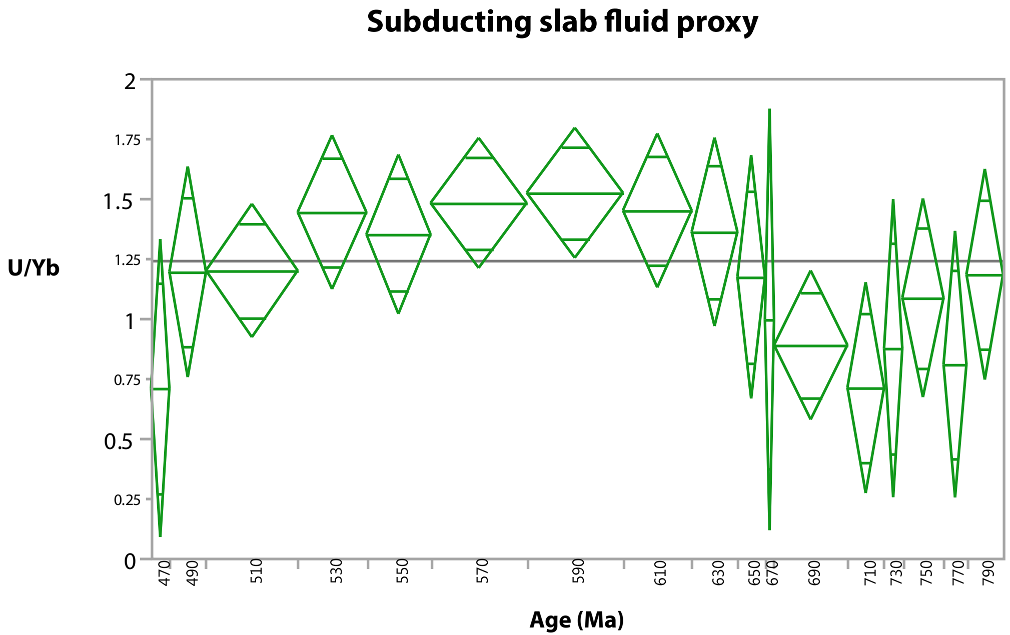

Summary of Fit

Rsquare	0.149283
Adj Rsquare	0.068742
Root Mean Square Error	0.629159
Mean of Response	1.241992
Observations (or Sum Wgts)	186

Analysis of Variance

Source	DF	Sum of Squares	Mean Square	F Ratio	Prob > F
Sample	16	11.739054	0.733691	1.8535	0.0281
Error	169	66.897146	0.395841		
C. Total	185	78.636201			

Supplementary Figure DR3.

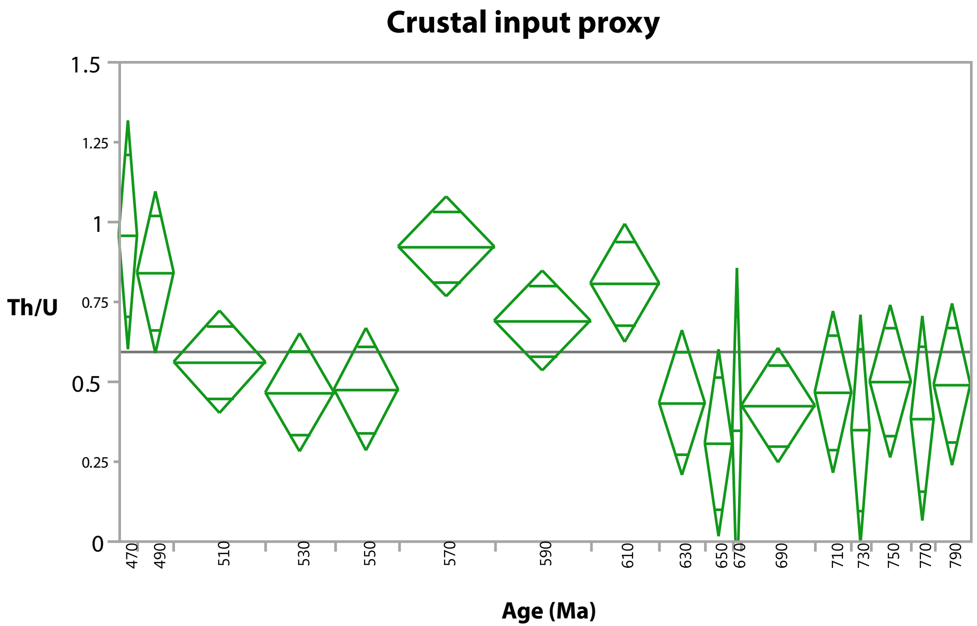

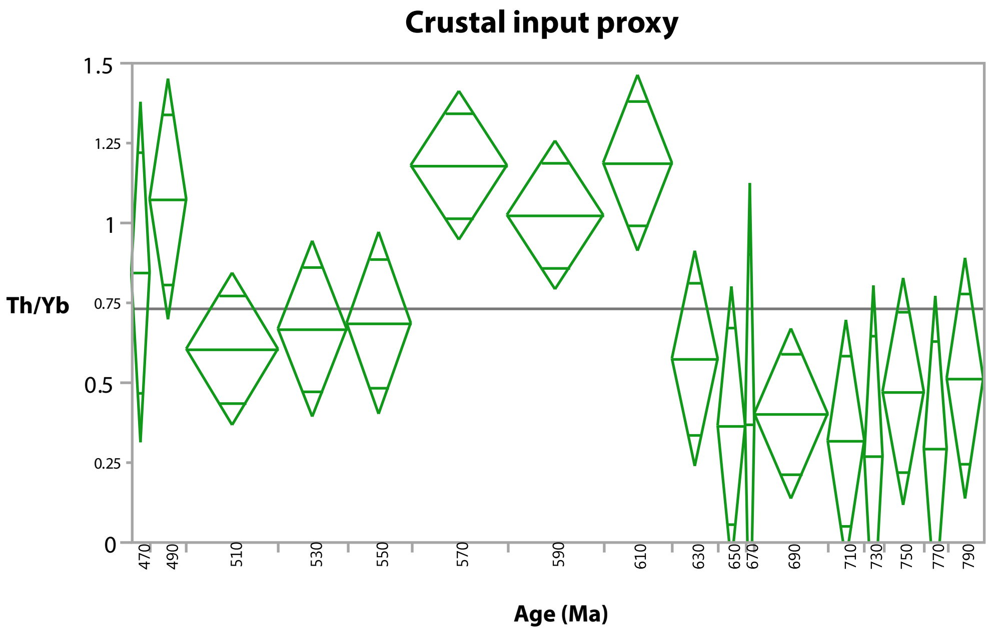

Summary of Fit

Rsquare	0.231635
Adj Rsquare	0.158891
Root Mean Square Error	0.362951
Mean of Response	0.593399
Observations (or Sum Wgts)	186

Analysis of Variance

Source	DF	Sum of Squares	Mean Square	F Ratio	Prob > F
Sample	16	6.711507	0.419469	3.1842	<.0001
Error	169	22.262926	0.131733		
C. Total	185	28.974432			

Summary of Fit

Rsquare	0.26473
Adj Rsquare	0.195118
Root Mean Square Error	0.539748
Mean of Response	0.731426
Observations (or Sum Wgts)	186

Analysis of Variance

Source	DF	Sum of Squares	Mean Square	F Ratio	Prob > F
Sample	16	17.726559	1.10791	3.8030	<.0001
Error	169	49.234420	0.29133		
C. Total	185	66.960979			

Supplementary Figure DR4.

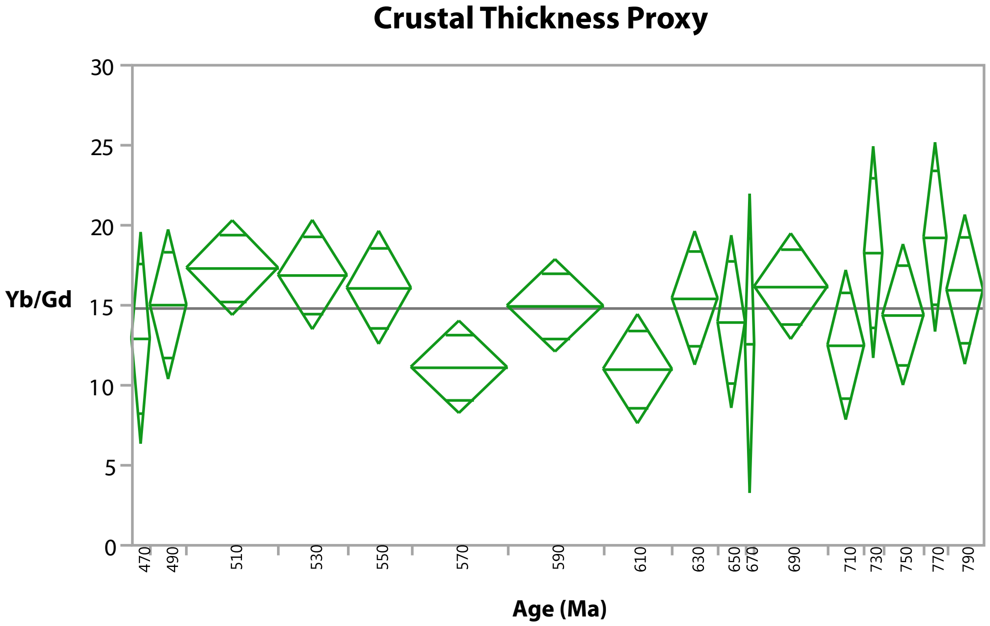

Summary of Fit

Rsquare	0.114512
Adj Rsquare	0.030679
Root Mean Square Error	6.699532
Mean of Response	14.80333
Observations (or Sum Wgts)	186

Analysis of Variance

Source	DF	Sum of Squares	Mean Square	F Ratio	Prob > F
Sample	16	980.9428	61.3089	1.3659	0.1641
Error	169	7585.3510	44.8837		
C. Total	185	8566.2938			

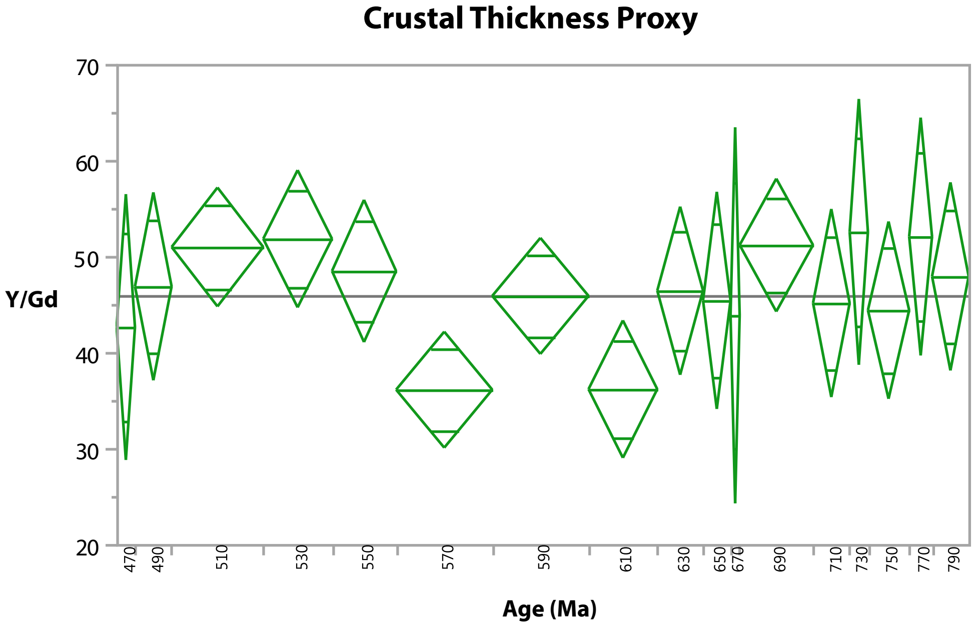

Summary of Fit

Rsquare	0.141908
Adj Rsquare	0.060669
Root Mean Square Error	14.02617
Mean of Response	45.92995
Observations (or Sum Wgts)	186

Analysis of Variance

Source	DF	Sum of Squares	Mean Square	F Ratio	Prob > F
Sample	16	5498.433	343.652	1.7468	0.0425
Error	169	33247.931	196.733		
C. Total	185	38746.364			